Mechanical and Electromechanical Coupling in Carbon Nanotube Distortions

Yu.N. Gartstein
Xerox Corporation, 147-59B, 800 Phillips Road, Webster, NY 14580

A.A. Zakhidov and R.H. Baughman
UTD NanoTech Institute, University of Texas at Dallas, Richardson, TX 75083

(Dated: September 10, 2002)

A simple approach is presented for an effective description of static deformations of carbon nanotubes in terms of bond-stretching and bond-bending modes and for actuation effects related to these deformations. The approach allows us to analyze various phenomena in a unified way and to clarify their relationships. We discuss the gap energy modulation by external strains, dimensional and torsional deformations caused by charge injection, and stretch-induced torsion. We show how symmetry determines dependence on the chiral angle of nanotubes. Particularly interesting are actuation responses that are caused by the modulation of electron kinetic energy by the deformations. Their strong oscillatory dependence on the nanotube geometry is explained within an intuitively clear bonding pattern picture. It is demonstrated how anisotropic (shear) deformations play an important role in nanotubes making their responses distinctly different from the graphite's.

PACS numbers: 61.46.+w, 73.22.-f, 71.38.-k, 85.85.+j

I. INTRODUCTION

Carbon nanotubes are particularly interesting nanoscopic systems[1] whose electronic and mechanical properties have been the subject of numerous studies and are attractive for diverse applications[2,3]. In this paper we study how microscopic displacements of atoms on a hexagonal atomic network of nanotubes provide for specific mechanical and electromechanical couplings that may be of interest for nanoactuators to convert between different types of energy. We will be discussing the deformations of nanotubes resulting from the charge injection as well as coupling between stretching and torsional deformations.

Electromechanical actuation using single-wall nanotubes (SWNTs) has been demonstrated in electrochemical cells[4]. Actuator strains of above 1% have been observed[3], which is about 10 times that of ferroelectrics, indicating the technological opportunity for direct conversion of electrical energy into mechanical. Currently available nanotube sheets and long fibers comprise bundles of SWNTs, each bundle containing from 30 to 100 of SWNTs of various internal geometries, or chiral vectors (N, M)[1]: from zigzag $(N, 0)$ to armchair (N, N) tubes. In a recent publication[5] we studied a simplified electron-lattice model at low injection levels and showed that SWNTs exhibit quite a unique picture of electromechanical actuation that strongly depends on (N, M) and the magnitude of the response of individual tubes, partucularly of semiconducting zigzags, can be appreciably larger than that of graphite. Here we extend that study on the basis of a more complete picture of elastic interactions and to include the torsional deformations. We also provide a simple bonding picture to explain the peculiar behavior of nanotube responses.

Stretch-induced torsion of SWNTs has been found in molecular dynamics simulations.[6] Here we present a theory of this effect showing that it is caused by the curvature-derived elastic anisotropy and that the maximum effect is expected for the chiral tubes in the middle between armchair and zigzag tubes. Although demonstrating an opportunity for converting tensile strain into torsion, the magnitude of the effect in carbon nanotubes may be small. We indicate that other nanotubes with inherent elastic anisotropy, such as BC_2N tubes[7], could provide a substantial advantage.

Our focus will be on a simple unified description of and relationships between various effects. The approach consists of finding the static lattice distortion patterns $\mathbf{D}$ that minimize the total adiabatic energy of the system per carbon atom:

$$E(\mathbf{D}) = U(\mathbf{D}) + E_{\rm el}(\mathbf{D}), \tag{1}$$

where U is the lattice elastic potential energy, including energies of all valence electrons of the *undoped* system, and $E_{\rm el}$ the energy of *extra* charges if δn electrons per atom have been added.

We find it convenient to discuss static distortions of nanotubes in terms of effective 2-d displacements of atoms of a parent graphene sheet out of which nanotubes are rolled.[1] Both bond-stretching and bond-bending displacements of the hexagonal atomic lattice are considered that can form *isotropic* and *anisotropic* distortion modes. The latter modes turn out to be intimately related to many interesting effects specific to nanotubes. Appropriate empirical expressions for U will be built that are based entirely on the symmetry requirements in the spirit of the continuum mechanics, and connections be established between the microscopic displacements picture and the macroscopically observable distortions (section II). For $E_{\rm el}$ we use a tight-binding model of π-electron bands[1] whose parameters can be affected by the lattice distortions (section III). When a strain is applied to the undoped system, the deformation $\mathbf{D}$ occurs so as to min-

imize U and this results in modulation of some electronic parameters, such as the gap energy[8] (section IV), and, possibly, in a strain "along another direction" (section VI). Conversely, if charges are added to the system, the lattice will try to accommodate them with the deformation $\mathbf{D}$ that minimizes E (section V). For illustrative purposes, some parameterization will be used to carry out numerical calculations.

II. MACRO- AND MICROSCOPIC 2-d DISTORTIONS

Elastic in-plane deformations of the graphene sheet provide a natural basis for the effective 2-d description of nanotube deformations. An arbitrary 2-d crystal structure may have many atoms in the unit cell (graphene has 2 atoms) and, correspondingly, many deformation degrees of freedom. From the standpoint of macroscopic distortions, however, "internal" degrees of freedom are disguised and the only static observable is the deformation of the unit cell as a whole or, alternatively, of the triangle built of the primitive lattice vectors and assumed periodically repeated. To specify the 2-d *deformation* of the triangle, one needs 3 parameters, precisely as many as is needed to specify the in-plane deformations of a 2-d elastic continuum. Let us choose a convenient 2-d system of coordinates with axes x and y (axes in Fig. 1 are related to the underlying hexagon structure). With overall translation and rotation excluded, a general linear deformation (displacement $(\delta x, \delta y)$ of the point (x, y)) of the elastic continuum can be described as

$$\begin{pmatrix} \delta x \\ \delta y \end{pmatrix} = \begin{pmatrix} \gamma_0 + \gamma_x & \eta_x \\ \eta_x & \gamma_0 - \gamma_x \end{pmatrix} \begin{pmatrix} x \\ y \end{pmatrix}. \qquad (2)$$

Parameter γ_0 here corresponds to isotropic distortions, while γ_x and η_x correspond to anisotropic distortions and are components of the pure shear strain tensor.

In nanotubes, there would also be another natural system of coordinates related to the nanotube axis (in Fig. 1 $x-$aixs is at angle $\phi > 0$ to the nanotube axis). With the coordinates rotated as

$$\begin{pmatrix} x_1 \\ y_1 \end{pmatrix} = \begin{pmatrix} \cos\phi & -\sin\phi \\ \sin\phi & \cos\phi \end{pmatrix} \begin{pmatrix} x \\ y \end{pmatrix}, \qquad (3)$$

γ_0 remains invariant while shear components are known to transform as

$$\begin{pmatrix} \gamma \\ \eta \end{pmatrix} = \begin{pmatrix} \cos 2\phi & -\sin 2\phi \\ \sin 2\phi & \cos 2\phi \end{pmatrix} \begin{pmatrix} \gamma_x \\ \eta_x \end{pmatrix}.$$

Macroscopic deformations of the tube as a whole are defined and measured with respect to the tube axis. The three parameters (γ_0, γ, η) translate into the observable longitudinal dimensional change $\delta L/L = \gamma_\parallel = \gamma_0 + \gamma$, transversal change $\delta R/R = \gamma_\perp = \gamma_0 - \gamma$, and the torsional deformation $\delta\phi_l = \eta/\pi R$ (the latter is in turns per unit length, R being the tube radius).

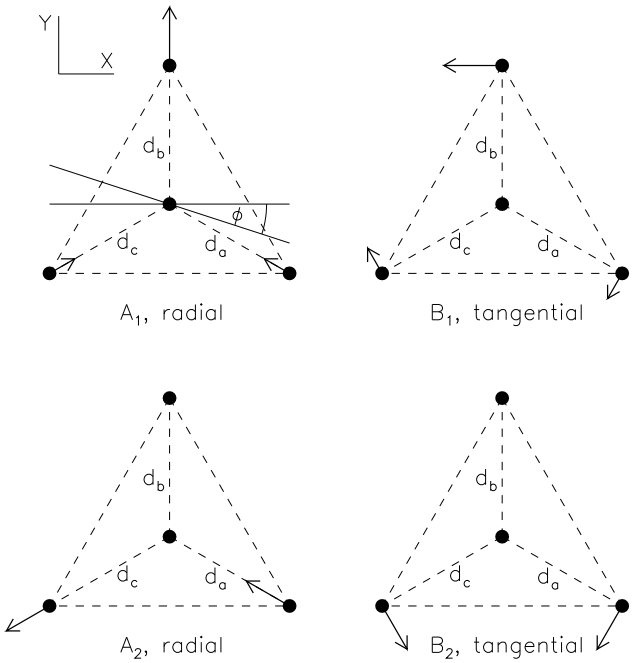

FIG. 1: Four carbon atoms of the repeating motive are depicted with the three types of bonds d_a, d_b, and d_c. In each of the four panels schematically shown are the carbon atom displacements corresponding to the defined anisotropic distortion modes. The nanotube axis is at the angle ϕ with $x-$axis.

For a full description of the 2-d deformation of the graphene unit cell with two atoms, one however needs 5 parameters. We consider the deformations in terms of radial (bond-stretching: δ_a, δ_b, δ_c for, respectively, bonds d_a, d_b, d_c) and tangential (bond-bending: r_a, r_b, r_c) displacements of carbon atoms, as should be clear from Fig.1. Let us express those displacements as linear combinations of the corresponding *isotropic* (S, Q) and *anisotropic* (A_1, A_2) and (B_1, B_2) distortion modes, e.g.:

$$\begin{aligned} \delta_a &= S/3 - A_1/2\sqrt{3} - A_2/2, \\ \delta_b &= S/3 + A_1/\sqrt{3}, \\ \delta_c &= S/3 - A_1/2\sqrt{3} + A_2/2, \end{aligned} \qquad (4)$$

for radial displacements and similarly for r_a, r_b, r_c through Q, B_1, B_2. It is clear, however, that the Q mode is not a deformation mode, it describes the overall rotation of the triangle irrelevant for our purposes and will be set $Q = 0$ in agreement with the definition (2). The 5 modes left can be used as convenient necessary 5 parameters. The isotropic mode S describes the overall size change of the triangle. The anisotropic distortions A_i and B_i result in triangle shape modifications as shown in Fig.1. It is also useful to introduce the rotated anisotropic deformation modes ($A_\parallel$, $A_\perp$) and ($B_\parallel$, $B_\perp$) defined with respect to the nanotube axis, they respectively relate to (A_1, A_2) and (B_1, B_2) as (x_1, y_1) to (x, y) in Eq.(3).

From Fig. 1 and from the corresponding definitions,

one can obtain the following compact expressions for the macroscopic deformations:

$$\begin{array}{lcl} d\cdot\gamma_0 &=& S/3, \\ d\cdot\gamma &=& (B-A)/2\sqrt{3}, \\ d\cdot\eta &=& (C-D)/2\sqrt{3}, \end{array} \tag{5}$$

where

$$\begin{array}{lcl} A &=& A_\parallel\cos 3\phi + A_\perp \sin 3\phi, \\ B &=& B_\parallel \sin 3\phi - B_\perp \cos 3\phi, \\ C &=& -A_\parallel \sin 3\phi + A_\perp \cos 3\phi, \\ D &=& B_\parallel \cos 3\phi + B_\perp \sin 3\phi. \end{array} \tag{6}$$

The length unit d above stands for the undeformed nearest neighbor carbon-carbon bond length, another length unit to be used is the second order carbon-carbon distance $a = d\sqrt{3}$. Notice that macroscopic results (5,6) are *invariant* with respect to rotation $\phi \to \phi + 2\pi/3$ as one should expect from the symmetry of the hexagon structure.

The elastic energy of the the in-plane deformations of the graphene sheet is invariant with respect to the rotation of the 2-d system of coordinates. Using all rotationally invariant combinations of the introduced deformation modes, the harmonic deformation energy per carbon atom can in general be written down as

$$\begin{array}{rcl} U^0 &=& \dfrac{K_S}{2}S^2 + \dfrac{K_A}{2}(A_\parallel^2 + A_\perp^2) \\ &+& \dfrac{K_B}{2}(B_\parallel^2 + B_\perp^2) + K_{AB}(A_\parallel B_\perp - A_\perp B_\parallel). \end{array} \tag{7}$$

It is up to *ab initio* and/or empirical models to establish numerical values of the elastic constants. In this paper, we will be using some estimates for illustrative purposes. For instance, a good representation of the elastic properties of graphene is believed to be achieved within an empirical force constant model including terms up to four near neighbor levels as described and referenced in Ref. 1. Using that model, one can express the elastic constants in (7) through the force constants $\phi_i^{(j)}$, e.g.:

$$K_S = \phi_r^{(1)}/6 + \phi_r^{(2)} + 2\phi_r^{(3)}/3 + 7\phi_r^{(4)}/3$$

for the S mode and so on. Then, using numerical values of the force constants quoted on p.169 of Ref. 1, one would arrive at the following magnitudes of the elastic constants (in eV/Å^2):

$$K_S = 7.74, \;\; K_A = 4.56, \;\; K_B = 7.14, \;\; K_{AB} = 1.21. \tag{8}$$

With these numbers, A_i modes turn out to be softer than B_i modes, and the coupling between A_i and B_j modes is relatively weak. It is useful to compare relative strengths in (8) to the nearest neighbor elastic spring model used in Ref. 5 where $K_S = K/6$ and $K_A = K/4$: evidently (8) yields relatively softer A_i modes as we indeed expected.

For a given macroscopic distortion (γ_0, γ, η) of the undoped sheet, the microscopic distortion modes adjust so as to minimize the microscopic energy (7). The resulting rotationally invariant *macroscopic* deformation energy per carbon is

$$U^0_{\rm m} = \frac{C_0}{2}\,\gamma_0^2 + \frac{C_{\rm sh}}{2}(\gamma^2 + \eta^2), \tag{9}$$

where the effective elastic energies $C_0 = 9d^2K_S$ and $C_{\rm sh} = 12d^2Z_{ab}/z_{ab}$.[19] When going from (7) to (9), one can also answer an interesting question as to when displacements of *all* atoms in the unit cell of graphene are such as if they were on a 2-d continuum. For this to happen, the optimal distortion modes should satisfy $A_\parallel = B_\perp$, $A_\perp = -B_\parallel$, requiring $K_A = K_B$. With numbers (8) and $d = 1.42$Å, the elastic energies $C_0 = 140.5$ eV, $C_{\rm sh} = 81.1$ eV. The effective 2-d Poisson ratio $\nu = (C_0 - C_{\rm sh})/(C_0 + C_{\rm sh})$ turns out to be 0.27, close to the earlier reported[9] value within the same force constant model, and the in-plane stiffness per carbon $C = C_0C_{\rm sh}/(C_0 + C_{\rm sh}) = 51.4$ eV.

When the graphene sheet is wrapped to form a carbon nanotube, the effective 2-d elastic description would undergo certain changes. From the results of *ab initio* calculations[10,11], it is known that even in the ground state of nanotubes the equilibrium bond lengths d_a, d_b, d_c can differ from each other and are different from the graphene bond length d. These effects can easily be absorbed in our description by thinking that the ground states of nanotubes are somewhat deformed (with respect to graphene). It should be understood that the deformation is in general anisotropic (the rotational invariance is lifted since a new selected direction would now exist – the nanotube axis). Using general symmetry considerations[20], one can show that the deformation of the ground state can be described by 3 R-dependent distortion parameters (S_R, A_R, B_R) so that

$$\begin{array}{ll} A_\parallel = A_R\cos 3\phi, & A_\perp = A_R \sin 3\phi, \\ B_\parallel = B_R \sin 3\phi, & B_\perp = -B_R\cos 3\phi. \end{array} \tag{10}$$

Note that (10) is required by the symmetry. That is, extraction of the functions (S_R, A_R, B_R) from *ab initio* data[10,11] for, say, armchair nanotubes would be sufficient to describe the deformed ground states for the tubes of arbitrary chirality. In this paper we do not pursue these numerical fits to the *ab initio* data.

When using the expression (7) for the elastic energy, we now understand that the deformation modes $S, A_\parallel, \ldots$ used there are calculated relative to their values in the corresponding ground states. In addition to this however, in nanotubes of a finite radius R, the curvature also modifies the very elastic couplings. First, the elastic constants K in (7) can be renormalized with corrections $\propto 1/R^2 + \ldots$ That is, all coefficients in (7,9) and quantities derived from them are in general R-dependent. Second, the rotational invariance of the elastic energy is also lifted. Using the same symmetry considerations[20], one can show that this axial symmetry breaking in the har-

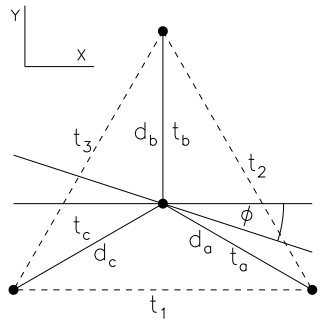

FIG. 2: NNH and SOH integrals, whose modulation is considered.

monic approximation will occur in the form $U = U^0 + \delta U$,

$$\begin{aligned}\delta U &= K^a_{SA} SA + K^a_{SB} SB + \frac{K^a_A}{2}(A^2_\parallel - A^2_\perp) \\ &+ \frac{K^a_B}{2}(B^2_\parallel - B^2_\perp) + K^a_{AB}(A_\parallel B_\perp + A_\perp B_\parallel), \quad (11)\end{aligned}$$

where definitions (6) have been used and anisotropy parameters $K^a \propto 1/R^2 + \dots$ For description of some of the effects, the isotropic deformation energy (7) is already sufficient, but for other, the elastic anisotropy expressed in Eq. (11) is essential, we resort a discussion to section VI.

III. SINGLE ELECTRON SPECTRUM

We consider the electron kinetic energy to arise both from nearest neighbor (NNH) and second order (SOH) hopping between carbon atoms as depicted in Fig.2. The hopping integrals are modulated by the lattice distortions providing thus the electron-lattice interaction. (An additional effect would e.g. follow from the modulation of Coulomb repulsion between extra charges.) As is customary, a linear modulation with distances is assumed. So NNH integrals are modulated as

$$t_a = t_0 - \alpha\delta_a, \quad t_b = t_0 - \alpha\delta_b, \quad t_c = t_0 - \alpha\delta_c, \qquad (12)$$

where t_0 is the NNH integral on the undistorted lattice and α the NNH coupling constant. Similarly, SSH integrals t_1, t_2, and t_3 are modulated with the SOH distances, the modulation strength given by the SOH coupling constant β. We expect $\beta/\alpha \sim 0.1$. Expressing changes of distances in terms of introduced distortion modes (4) will yield the corresponding coupling constants for each of the modes as used below. With SOH included, the charge conjugation symmetry (CCS) of the half-filled system is broken and the band energies have the form

$$\epsilon_\pm(\vec{k}) = \tau(\vec{k}) \pm \xi(\vec{k}) \qquad (13)$$

for the conduction and valence bands, respectively, where $\xi(\vec{k})$ originates from the NNH and $\tau(\vec{k})$ from the SOH, and $\vec{k} = (k_x, k_y)$ is the 2-d dimensional wavevector. With the definitions of Fig.2,

$$\begin{aligned}\tau(\vec{k}) &= -2t_1 \cos k_x a - 2t_2 \cos k_- a \\ &- 2t_3 \cos k_+ a, \qquad (14)\\ \xi^2(\vec{k}) &= t_a^2 + t_b^2 + t_c^2 + 2t_a t_c \cos k_x a + 2t_a t_b \cos k_- a \\ &+ 2t_b t_c \cos k_+ a, \qquad (15)\end{aligned}$$

where $k_\pm = (k_x \pm \sqrt{3}k_y)/2$. For not too small nanotubes the low excitation energy region is always close to the special, "Dirac", points in the momentum space, where the gap between the valence and conduction states of the (isotropic) graphene spectrum (as determined by (15)) vanishes. Then one can use expansions of the exact band energies (14, 15) in momenta around the special points and in (small) deviations of hopping integrals around their bare values. For certainty, we choose the special point $\vec{K} = (4\pi/3a, 0)$ and from now on, all momenta $\vec{k} = (k_x, k_y)$ will be measured with respect to that special point ($k_x \to 4\pi/3a + k_x$). After some exercise, one reduces (14, 15) to

$$\begin{aligned}\tau(\vec{k})/t_0 &= \tau_0(\vec{k})/t_0 + \sqrt{3}(\beta/\alpha)\Big(\hat{S} \\ &+ 3[k_x(\hat{A}_1 + \hat{B}_2) + k_y(\hat{A}_2 - \hat{B}_1)]a/4\Big), \quad (16)\\ \xi^2(\vec{k})/t_0^2 &= (3 + 2\hat{S} - 2\sqrt{3}\hat{A}_1)(k_x a - \hat{A}_1)^2/4 \\ &+ (3 + 2\hat{S} + 2\sqrt{3}\hat{A}_1)(k_y a - \hat{A}_2)^2/4 \\ &+ \sqrt{3}\hat{A}_2(k_x a - \hat{A}_1)(k_y a - \hat{A}_2). \qquad (17)\end{aligned}$$

Here τ_0 is the equilibrium value of τ and we introduced dimensionless variables $\hat{S} = -\alpha S/t_0$, $\hat{A}_1 = -\alpha A_1/t_0$, $\hat{A}_2 = -\alpha A_2/t_0$, $\hat{B}_1 = -\alpha B_1/t_0$ $\hat{B}_2 = -\alpha B_2/t_0$ to save space in formulae (the same would be used for rotated modes $A_\parallel$, $A_\perp$. Applicability of the expansions (16,17) requires $k_x a \ll 1$ and $k_y a \ll 1$ as well as relatively small distortion amplitudes. In view of this and of the smallness of β/α, one can safely neglect the terms in (16) that are proportional to $ka \ll 1$.

For the (N, M) tube, the chiral angle ϕ (Figs. 1, 2) is defined through $\sin\phi = (N-M)/2C_h$, where the dimensionless tube circumference $C_h = \left(N^2 + M^2 + NM\right)^{1/2}$ (it is related to the tube radius as $2\pi R = aC_h$). We consider ϕ belonging to the interval between 0 (armchair tubes) and $\pi/6$ (zig-zag tubes). The angle ϕ is complementary to the chiral angle θ as defined in Ref. 1: $\phi = \pi/6 - \theta$. Of extreme importance is the divisibility of $N - M$ by 3, the "remainder" $q = 0, \pm 1$ is introduced by

$$N - M = 3m + q, \qquad (18)$$

where m is the appropriate integer. The electron momenta can lie only on a set of quantization lines, the one most closely approaching the special point is described by

$$k_x \sin\phi + k_y \cos\phi = -2\pi q/3C_h a = K_0/a. \qquad (19)$$

According to (17), the lowest $\xi-$energy in the equilibrium system is $\xi_0 = t_0\left(3K_0^2/4\right)^{1/2} = |q|t_0 d/2R$, finite for semiconducting nanotubes ($|q| = 1$) and zero for metallic ones ($q = 0$).

One-dimensional (momentum k) "$\xi-$bands" along the quantization lines are obtained from (17) and have the familiar Dirac form

$$\xi^2(k) = \Delta^2 + v_\parallel^2 k^2, \tag{20}$$

where the gap parameter

$$\Delta = v_\perp |K_0 - \hat{A}_\perp|/a \tag{21}$$

and the effective Fermi velocities

$$v_\parallel = v_F - at_0\hat{A}/2, \qquad v_\perp = v_F + at_0\hat{A}/2. \tag{22}$$

Here $v_F/at_0 = \sqrt{3}/2 + \hat{S}/2\sqrt{3}$ and dimensionless $\hat{A}$ is defined through dimensionless $\hat{A}_\parallel$, $\hat{A}_\perp$ as in (6). Higher lying energy bands are evidently also described by (21) where q used in the definition of K_0 would be "displaced" by $3m$ where m is an integer. If, e.g., the lowest energy band corresponds to $q = -1$, the first higher lying band would be with $q = 2$, still the next with $q = -4$ and so on.

The curvature affects the effective 2-d description of the electron spectrum of nanotubes. As we discussed in section II, even in the ground states, nanotubes are deformed with respect to graphene. In our applications, it means that all distortion modes in Eqs. (16,17) and further on would have to be displaced like $S \to S_R + S$, $A_\parallel \to A_R \cos 3\phi + A_\parallel$, etc. In addition, the curvature changes the overlap of π-orbitals which can be represented as another source of the effective external distortion $A_R \to A_R + A_e$, $S_R \to S_R + S_e$, $S_e = \sqrt{3}A_e$, so that bonds along the tube axis do not change while the other bonds change their length appropriately. An elegant analysis of the modulation of the NNH by curvature was, e.g., given by Kane and Mele,[12] from their work we deduce the value $A_e = t_0\pi^2/4\sqrt{3}\alpha C_h^2$. In our calculations below, we will be taking into account only the anisotropy term A_e as responsible for curvature-derived gaps in quasi-metallic tubes.

IV. MODULATION OF THE GAP BY DEFORMATIONS

Modulation of the gap energy $E_g = 2\Delta$ by the longitudinal $\gamma_\parallel$ and torsional η strain is the effect whose extensive analysis was given in Ref. 8 where references to the earlier work can also be found. Here we discuss it within our framework indicating the differences with the treatment of Ref. 8 as well as giving a simple physical picture for the peculiar features of the effect.

Eq. (21) shows how the gap parameter Δ is modulated by the bond-stretching modes $S, A_\parallel, A_\perp$. When strains $\gamma_\parallel$ and/or η are applied, they cause the lattice distortions so as to minimize the elastic energy (7): in general both bond-stretching and bond-bending modes are excited but the latter do not affect the gap. The isotropic displacements are simply determined by $S = 3\gamma_0 d$, while anisotropic are related to the shear strain components:

$$\begin{aligned} A_\parallel &= -\sqrt{3}z_a(\gamma\cos 3\phi + \eta\sin 3\phi)d, \\ A_\perp &= -\sqrt{3}z_a(\gamma\sin 3\phi - \eta\cos 3\phi)d. \end{aligned} \tag{23}$$

Using equilibrium $\gamma_0 = (1-\nu)\gamma_\parallel/2$ and $\gamma = (1+\nu)\gamma_\parallel/2$, it is now straightforward to find the gap modulation δE_g of semiconducting tubes ($q = \pm 1$) at small strains:

$$\frac{\delta E_g}{\alpha d} = \frac{\pi(\nu - 1 + (1+\nu)z_a)}{\sqrt{3}C_h}\,\gamma_\parallel \tag{24a}$$

$$+\ 3qz_a\left[(1+\nu)\gamma_\parallel\sin 3\phi - 2\eta\cos 3\phi\right]/2. \tag{24b}$$

Apart from the difference in notation, (24b) agrees with the result of Ref. 8 on the chiral dependence of the major modulation effect. Noteworthy is the appearance of the factor z_a in (23,24), which would be 1.28 with numbers (8). Analytical calculations of Ref. 8 assume the lattice to deform under the strain as if it was a 2-d elastic continuum. The factor z_a accounts for the difference caused by the actual elastic properties of the lattice, this factor becomes unity[19] when the difference effectively disappears. In the extreme case of $K_B = K_{AB} = 0$, the factor z_a becomes 0, and the largest part of the gap modulation (24b) disappears because the shear deformation would be realized only through the bond-bending modes. In the opposite extreme case of $K_B = \infty$, all the shear occurs through bond-stretching modes and the factor $z_a = 2$. Ref. 8 provides numerical results on modulation for a specific choice of the coupling constant α. Eq. (24a) reflects a correction $\propto 1/R$ coming from the modulation of the Fermi velocity in (21).

The notable feature of Eq. (24b) is the factor q which leads to responses of the semiconducting tubes oscillating as a function of $N - M$. Consider, e.g., zigzag tubes that have the strongest response to the longitudinal strain. The longitudinal expansion of the (10, 0) tube with $q = 1$ results in the gap increase while the expansion of the (11, 0) tube with $q = -1$ in the gap decrease. We find that a very transparent physical picture can be offered to understand this fascinating behavior. Let us calculate the contributions to the gap energy of the semiconducting tubes

Tube	d_a	d_b	d_c	Δ/t_0
(10,0)	-1.0	0.588	0.588	0.176
(11,0)	1.0	-0.415	-0.415	0.169
(10,5)	0.954	-0.1	-0.715	0.139
(10,6)	-0.916	0.227	0.818	0.128

TABLE I: The bonding patterns for four tubes. The contributions from bonds d_a, d_b and d_c are normalized so that their sum gives the gap parameter in units of t_0.

coming from different types of nearest neighbor carbon-carbon bonds, i.e., the matrix elements of the corresponding parts of the Hamiltonian at the conduction band minimum wave vectors ($k_x a = K_0 \sin\phi,\ k_y a = K_0 \cos\phi$, see (19)). The problem is equivalent to finding the phase factors for three vectors representing the three types of bonds that maximize the conduction-valence band splitting. One readily derives that the bonds d_i contribute $-\cos(\varphi + \phi_i)$ to Δ/t_0 , where $\varphi = -q\pi/2 - \phi$, $\phi_a = 2\pi/3 + K_0 \sin(\phi - \pi/6)/\sqrt{3}$, $\phi_b = K_0 \cos\phi/\sqrt{3}$, and $\phi_c = -2\pi/3 - K_0 \sin(\phi + \pi/6)/\sqrt{3}$. Table I gives numerical examples of the bond contributions for four tubes. We will call "bonding" those bonds whose contribution is negative and "antibonding" those whose contribution is positive. By definition, expansion of the bonding bonds increases the gap, and their contraction decreases the gap; effects for the antibonding bonds are opposite. Table I illustrates a dramatic difference of the bonding patterns of tubes with $q = 1$ and $q = -1$. And, indeed, the bond d_a along the tube axis of the zigzag tubes turns out to be bonding for the (10, 0) tube but antibonding for the (11, 0) tube, leading to effects in agreement with (24b). By the same token, it is clear that a twist of a certain direction would result in opposite effects on the gap for tubes (10, 5) and (10, 6).

For quasi-metallic tubes ($q = 0$), the gap modulation is given by $\delta E_g = \sqrt{3}\alpha s_0 A_\perp$, where $s_0 = \mathrm{sign}(A_e \sin 3\phi + A_\perp)$ with $A_\perp$ from (23) and $\gamma = (1 + \nu)\gamma_\parallel/2$. In the absence of the curvature-induced gap ($A_e \sin 3\phi = 0$), of course, strains could only produce a finite gap. With the curvature-derived gap in place, there would be a range of relatively small strains where the gap can be decreased. We note that a small longitudinal expansion $\gamma_\parallel > 0$ particularly leads to such an effect. It is intuitively clear: the curvature makes hopping integrals "perpendicular" to the tube axis smaller than those "parallel" to the axis. The curvature-derived gap would be decreased if all the hopping integrals become more equilibrated, and for this one needs a longitudinal expansion and/or transversal contraction.

V. CHARGE-INDUCED DISTORTIONS

Suppose one adds δn extra electrons ($\delta n < 0$ for holes) per carbon atom to a SWNT. How would interatomic distances be affected? Here we study the contribution to bond length changes arising from the modulation of electron hopping integrals t by lattice distortions. The basic illustration is very simple: if an extra electron or hole is added to a half-filled two-site system, this would cause an expansion of the inter-site bond by $\delta d = \alpha/K$, where K is the elastic constant and the hopping integral is modulated as $\delta t = -\alpha\delta d$. We will show that this relaxation mechanism can produce surprisingly different results for carbon nanotubes having different values of N and M.

To evaluate the lattice deformation to accommodate additional charges on the nanotube, we need to know the energy $E_{\rm el}$ of extra charges as a function of the distortion coordinates. It is well known that one-dimensional electron-phonon systems can be unstable with respect to the Peierls distortion and exhibit formation of non-uniform polaronic distortions. For *not very small* carbon nanotubes, however, these effects seem practically irrelevant. The estimated transition temperatures (e.g. Ref. 13) and polaron binding energies[13,14] are on the order of 1K or smaller. So even quite low temperatures in excess of those estimates are sufficient to prevent non-uniform charge distributions. Of course, quantum fluctuations also act to render polaronic states unstable. With a uniform distribution of excess charges over the lattice sites and relatively low temperatures, it will be safe to assume that electrons/holes added to the system are accommodated in the band states of the lowest available excitation energies. The lattice displacements affect $E_{\rm el}$ through the variation of the band parameters as was discussed in section III.

With only one (with account of degeneracy) electronic band being filled, the variable part of the electronic energy per carbon takes the form

$$E_{\rm el} = \sqrt{3}(\beta/\alpha) S \delta n + (1/f) \int_0^{\delta k} \xi(k) \mathrm{d}k, \qquad (25)$$

where only one practically non-negligible term from (16) is left. The coefficient f relates the boundary δk of the occupied states in the momentum space to the charge injection level: $\delta k = f|\delta n|,\ f = \pi C_h/a\sqrt{3}$.

The lattice energy is given by (7), and the resulting distortion pattern is obtained by minimization of the total energy (1). Eq. (25) is independent of B_i distortion modes which then acquire a finite value only through the elastic coupling to A_i modes in (7). Substituting those derived values in (7) then leads to the effective lattice potential energy in terms of S and A_i modes only:

$$U = K_S S^2/2 + K'_A (A_\parallel^2 + A_\perp^2)/2 \qquad (26)$$

where $K'_A = K_A - K_{AB}^2/K_B$. With parameters (8), $K'_A = 4.35$ eV/Å^2. The dimensional changes (5) then would be

$$d \cdot \gamma = -uA/2\sqrt{3}, \quad d \cdot \eta = uC/2\sqrt{3} \qquad (27)$$

where the correction factor $u = 1 - K_{AB}/K_B = 0.83$ if (8) is used.

As an instructive example, we first analyze the effects linear in δn. Then the second term in (25) reduces to $\Delta|\delta n|$. Let us neglect all the curvature effects for this illustration. Minimization of the total energy is trivial and yields the optimal distortion pattern

$$\frac{K_S S}{|\delta n|} = \pm\sqrt{3}\beta + \frac{\pi\alpha|q|}{3\sqrt{3}C_h} \qquad (28a)$$

$$\frac{K'_A A_\parallel}{|\delta n|} = \frac{\pi\alpha|q|}{3C_h}\cos 3\phi \qquad (28b)$$

$$\frac{K'_A A_\perp}{|\delta n|} = \frac{\pi\alpha|q|}{3C_h}\sin 3\phi + \sqrt{3}\alpha q/2. \qquad (28c)$$

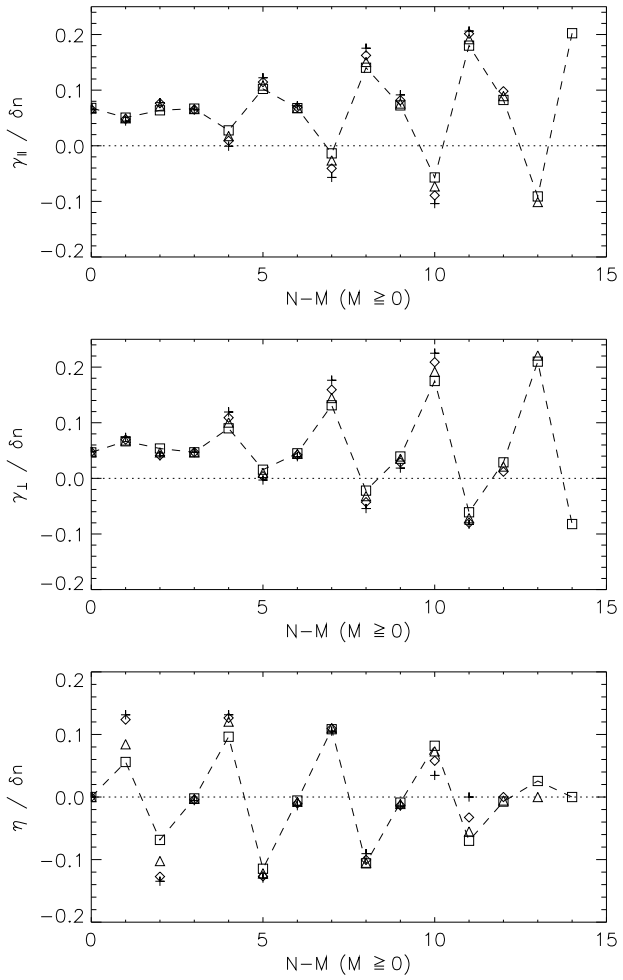

FIG. 3: Deformations of nanotubes for the electron doping level $\delta n = 0.5\%$. Shown are results for 4 "families" of carbon nanotubes: with $N = 11$ (crosses), 12 (diamonds), 13 (triangles), and 14 (squares). Connected with broken lines are the square data points. The upper panel shows changes in the nanotube length, the middle shows changes in nanotube radius and the lower panel torsional shear.

This corresponds to the following macroscopic distortions:

$$\gamma_0 = \frac{1}{\sqrt{3}K_S d}\left(\pm\beta + \frac{\pi\alpha|q|}{9C_h}\right)|\delta n|, \quad (29a)$$

$$\gamma = -\frac{u\alpha}{4K'_A d}\left(\frac{\pi|q|}{6\sqrt{3}C_h} + q\sin 3\phi\right)|\delta n|, \quad (29b)$$

$$\eta = \frac{u\alpha}{4K'_A d}\, q\cos 3\phi\ |\delta n|, \quad (29c)$$

upper/lower signs in (28,29) stand for electron/hole doping.

Of course, the most interesting are the proportional to q terms in (29b,29c) that lead to responses oscillating as a function of $N - M$. For semiconducting tubes, these terms are dominating, and they establish a large scale anisotropy of the axial ($\gamma_\parallel = \gamma_0 + \gamma$) and radial ($\gamma_\perp = \gamma_0 - \gamma$) responses. The electron-hole symmetric effect here is inverse to the gap modulation effect discussed in the previous section: extra charges at the band extremum want to decrease their energy by decreasing the gap. The bonding picture illustrated in Table I helps understand the peculiar oscillations and anisotropy. So for the (10,0) tube ($q = 1,\ 3\phi = \pi/2$) the bonds along the tube axis are bonding, they therefore shrink upon charge injection. The bonds "perpendicular" to the tube axis are antibonding and they would expand. This picture reverses for the tube (11,0) with $q = -1$, in full agreement with (29b). We note that these peculiar effects in (29b,29c) result exclusively from the excitation of the $A_\perp$ mode (28c) that directly modulates the gap (21).

Figure 3 displays equilibrium deformations of a series of nanotubes for the electron doping level $\delta n = 0.5\%$ calculated through a numerical optimization of the total energy. The figure shows not only the linear effects (29) but also the interplay of effects coming from the curvature and from the filling of the electron states above the band edge. Appearance of a small gap $\propto A_e$ drastically changes the responses of quasimetallic nanotubes for very low doping levels. However, the role of a small gap quickly diminishes upon increase of the doping level. For calculations, in addition to the elastic constants (8), we used electronic parameters: $\alpha = 5$ eV/Å and $\beta/\alpha = 0.2$. The results are practically independent of the value of t_0. The salient qualitative features: an oscillating character of the responses as a function of the nanotube geometry and a large scale anisotropy of the dimensional changes, are clearly seen.

Further increase of the injection level leads to charges starting to fill in the higher lying energy bands. The lowest critical densities are found as $\delta n_{\rm met} = 2\sqrt{3}/C_h^2$, $\delta n_{\rm sem} = 2/C_h^2$. This yields, e.g., $\delta n_{\rm met} \simeq 1.2\%$ for the (10, 10) nanotube, and $\delta n_{\rm sem} \simeq 1.7\%$ for the (11, 0) nanotube. Onset of the filling in the next higher lying bands leads to sudden changes in the responses – obviously, a distortion $A_\perp$ that decreases the gap (21) for the first band (say, with $q = 1$) would increase the gap for the second band (with $q = -2$). "Conflict of interests" of different bands is studied with the single band integral in Eq.(25) replaced with $\sum_i \int_0^{\delta k_i} \xi_i(k)\mathrm{d}k$ over multiple bands i with appropriate boundaries δk_i. In Figure 4 we show calculated $\gamma_\parallel$ for a series of carbon nanotubes as a function of the injection level. Sharp changes in the responses are clearly seen for the tubes (16, 0) and (17, 0), whose critical densities are within the displayed injection range.

Within the same model, the dimensional response of graphite would be a smooth curve[21]

$$\gamma_0 = \frac{1}{\sqrt{3}K_S d}\left[\beta\delta n + \alpha\frac{2}{\pi}\left(\frac{\pi|\delta n|}{3\sqrt{3}}\right)^{3/2}\right], \quad (30)$$

while $\gamma = \eta = 0$. In graphite, it is only the isotropic mode that gets excited upon charge injection leading to the isotropic expansion/contraction of the lattice. The

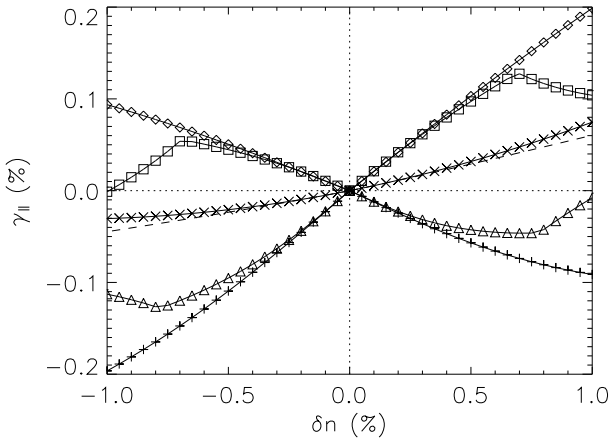

FIG. 4: Longitudinal dimensional changes for a series of doped nanotubes as a function of the injection level. Positive δn correspond to electron doping and negative to hole. Crosses are for the (10, 0) zig-zag tube, diamonds for the (11, 0) tube, triangles for the (16, 0) tube, squares for the (17, 0) tube, and x's for the (10, 10) armchair tube. Lines just connect the calculated data points. The dashed line shows the result (30) for graphite.

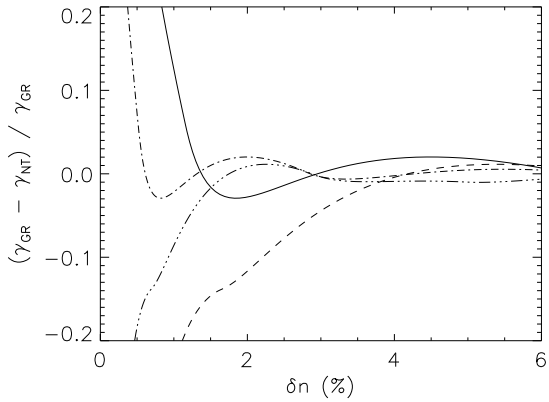

FIG. 5: Relative deviations of the isotropic NNH part of nanotube responses ($\gamma_{\rm NT}$) from that of graphite ($\gamma_{\rm GR}$) as a function of the charge injection level. Shown are results: with the solid line for the (10, 10) tube, dashed for the (11, 0) tube, dash-dotted for the (15, 15) tube, and dash-dot-dotted for the (17, 0) tube.

second order effect $\propto \beta$ in (30) provides for CCS breaking between electron and hole doping, and is the same as in the nanotubes independently of their geometry (29a). This term is important to account for electron-hole doping asymmetry of graphite intercalation compounds, as has been suggested in earlier work[11,15,16]. Experiments on electrochemical actuators with carbon nanotubes[4] also indicated an asymmetric response. Being linear in the doping concentration δn, this term can be dominating for graphite and quasimetallic tubes with $q = 0$ (at least for the armchair tubes). Strong electron-hole asymmetry of the graphite and armchair nanotube responses caused by the modulation of SOH is clearly seen in Figure 4.

On the other hand, the electron-hole symmetric NNH modulation (modulation of the Fermi velocity) in graphite results in the second term in (30) $\propto \alpha$. Similar isotropic parts are also present in the nanotube responses (see e.g. the second term in (29a)). They however have different functional dependence on δn. It is interesting to see how those parts converge to $\propto |\delta n|^{3/2}$ behavior of the graphite with increasing doping and/or with increasing nanotube size. Figure 5 illustrates this convergence as relative deviations of the corresponding parts of the responses. In fact, there are two universal behaviors there: one for metallic tubes and one for semiconducting, the curves within each class transform into each other with δn scaling as C_h^{-2}, where C_h is the tube circumference.

Of course, much larger deviations from the graphite behavior can occur due to anisotropic modes. These take place even for metallic tubes but, for semiconducting tubes at low doping levels, the electron-hole symmetric NNH gap modulation is especially significant leading to dimensional responses that can be substantially larger than graphite's. The nanotube strains caused by charge injection may generally be thought of as "fluctuating around" the graphite response, exhibiting the sharp transitions described above. The amplitude of the fluctuations and the spacing between them decrease with the size of the nanotubes, gradually approaching the graphite response as $N, M \to \infty$. With the increasing injection level, relative deviations from the graphite curve also become smaller.

It is the quantization of electronic states in nanotubes that makes anisotropic distortion modes a prominent feature of the accommodating lattice relaxation. Excitation of the anisotropic distortion modes causes the macroscopic shear deformations. The anisotropy of the longitudinal and transversal responses of nanotubes is one consequence, the other is the torsional deformations. At very low injection levels, the behavior of the latter is shown in Eq. (29c), numerical results for higher doping levels in Figures 3 and 6. As we discussed, onset of filling in higher energy bands causes sudden changes in responses, clearly seen in Figure 6 for twisting deformations.

For numerical calculations in this paper, we chose to increase parameter β/α because of the increased stiffness K_S, as compared to parameters used in Ref. 5, and in order to keep the results for graphite closer to experimental data (see, e.g., a compilation in Ref. 11). Of course, numerically results are affected by the choice of parameters, however the salient qualitative features distinguishing the behavior of nanotubes from graphite are quite robust. We hope that a more accurate parameterization of the model can be achieved by fitting to results of *ab initio* calculations such as in Ref. 11 and to experimental data, which is not attempted here.

The behavior discussed above arises at low temperatures in the single-electron picture. Thermal excitation of charges into higher lying energy bands will likely be bringing nanotube responses closer to the graphite's.

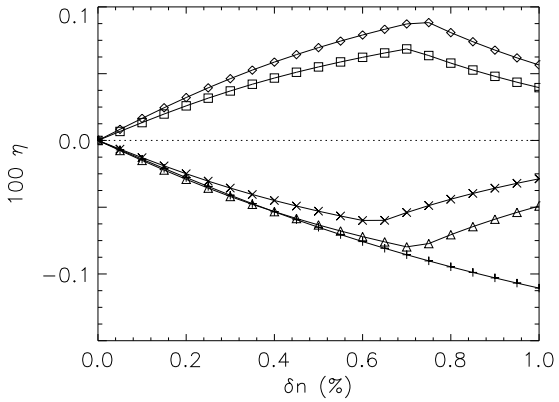

FIG. 6: Torsional shear deformations for a series of electron doped chiral semiconducting nanotubes as a function of the injection level. Crosses are for the (10, 5) tube, diamonds for the (10, 9) tube, triangles for the (12, 7) tube, squares for the (13, 6) tube, and x's for the (14, 6) tube. Lines here just connect the calculated data points.

However, since the separation between energy bands is large compared with the room temperature thermal energies for not too large tubes, we expect the thermal corrections to be small in such cases. Also, superimposed on the discussed effects can be a uniform expansion $\propto \delta n^2$ coming from the Coulomb repulsion of extra charges, whose magnitude depends on the positioning of counterions and dielectric properties of the medium. Coulombic intra-tube repulsion may dominate actuation when charge injected is large. This repulsion will however be absent in the system where extra electrons and holes are introduced as a result of photoexcitation and then quickly relax to the band edges and spend some time there. Evaluation of the $e-e$ correlation effects would require further studies, such effects may turn out unimportant for semiconducting nanotubes.

VI. STRETCH-INDUCED TORSION

In this section we deal with purely mechanical coupling – conversion of the tensile strain into torsion[6], the effect very familiar for ordinary helical springs. In our effective 2-d treatment, the tensile longitudinal deformation is described by the strain $\gamma_\parallel$ and the torsion $\delta\phi_l = \eta/\pi R$ by the η component of the shear tensor. The problem of the stretch-induced torsion can then be posed as finding the equilibrium η for a given $\gamma_\parallel$. It is quite clear that in an isotropic system with rotationally invariant elastic energy (9), the resulting optimal deformation for a given $\gamma_\parallel$ would have $\eta = 0$ and the stretch-induced torsion would not occur in the corresponding tube. The effective 2-d system has to be *anisotropic* for the optimal η not to vanish. Also, the system has to have lifted the reflection symmetry around the nanotube axis: $U_{\rm m}(\gamma_0,\gamma,\eta) \neq U_{\rm m}(\gamma_0,\gamma,-\eta)$, we can relate this to *chirality* of the system. Nanotubes readily give examples of such systems.

Two main questions to be clarified are: 1) How does η depend on the tube radius R? – General scaling arguments for not too small tubes with short-range elastic interactions require η to be an even function of $1/R$: $\eta = \eta_0 + \eta_2/R^2 + \eta_4/R^4 + \ldots$; η_0 here reflects the magnitude of the bare elastic anisotropy of the unwrapped sheet and equals to zero when the latter is elastically isotropic, while $\eta_2,\ \eta_4, \ldots$ are curvature derived effects.[22] Correspondingly, the large$-R$ scaling for the systems with bare anisotropy (like type-II BC_2N tubes[7]) is $\delta\phi_l \propto 1/R$ and for the systems with curvature-derived anisotropy (like carbon nanotubes) is $\delta\phi_l \propto 1/R^3$.[23] 2) How does η depend on the relative orientation of the tube axis, or on the chiral angle ϕ? – This dependence relates to the symmetry properties of the unwrapped sheet and/or to the symmetry breaking introduced by the wrapping.

Let us study the latter for carbon nanotubes. One can use the optimized microscopic distortions for a given macroscopic deformation (γ_0,γ,η) to derive the following macroscopic elastic anisotropy per carbon from (11):

$$\delta U_{\rm m} = C_0^a\gamma_0\gamma + \frac{C_{\rm sh}^a}{2}\left[(\gamma^2-\eta^2)\cos 6\phi + 2\gamma\eta\sin 6\phi\right]. \tag{31}$$

The functional form (31) is required by the symmetry of the axial anisotropy on a hexagonal background and can be also obtained directly using the same symmetry considerations.[20] Note that five anisotropy parameters of (11) have been reduced to only two. For small anisotropy, the effective anisotropy energies are found as $C_0^a = 3d^2(z_bK_{SB}^a - z_aK_{SA}^a)$ and $C_{\rm sh}^a = 3d^2(z_a^2K_A^a - z_b^2K_B^a + 2z_az_bK_{AB}^a)$. Both energies are curvature-derived and scale as $1/R^2 + \ldots$.

Optimizing $U_{\rm m} = U_{\rm m}^0 + \delta U_{\rm m}$ for a given $\gamma_\parallel$ and small anisotropy, we find the equilibrium η shear as

$$\eta/\gamma_\parallel = -(1+\nu)C_{\rm sh}^a\sin 6\phi/2C_{\rm sh}. \tag{32}$$

Eq. (32) indicates that maximum torsion for tubes of the same radius occurs at the chiral angle $\phi = \pi/12$, in the middle between armchair and zigzag tubes, and vanishes for achiral tubes, in agreement with results of molecular dynamics simulations.[6]

We now want to relate the curvature-derived stretch-induced torsion in (32) to another effect, the chirality dependence of the stiffness of nanotubes that was discussed in Refs. 10,17. With the same $U_{\rm m}$ we calculate anisotropy corrections to the longitudinal stiffness as

$$\frac{\partial^2 U_{\rm m}}{\partial\gamma_\parallel^2} = C + \frac{(1-\nu^2)}{2}\,C_0^a + \frac{(1+\nu)^2}{4}\,C_{\rm sh}^a\cos 6\phi, \tag{33}$$

where C is the contribution coming from $U_{\rm m}^0$ and discussed in section II. All C-energies in (33) are R-dependent. The coefficient $C_{\rm sh}^a$ in (33) that provides for a chirality dependence is the same that determines the torsional shear in (32). Eq. (33) predicts a monotonic dependence of the stiffness on the chiral angle between 0 and

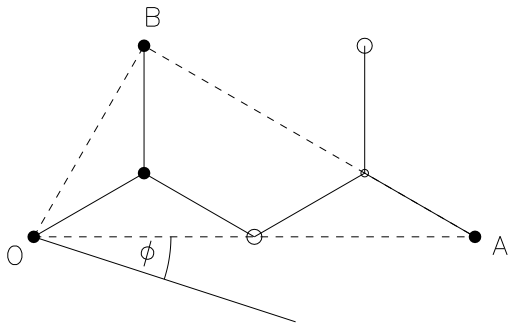

FIG. 7: Element of the type-II BC_2N tube structure with 4 atoms in the unit cell. Different circles denote different atoms. See Ref. 7 for details of the full structure.

$\pi/6$, which was indeed found in empirical calculations.[17] Comparing (33) to results of Ref. 17, we conclude that $C^a_{\rm sh} > 0$ and is substantial in the sense that its magnitude is comparable to the overall R-dependence of the longitudinal stiffness. The absolute magnitude of the effect however may strongly depend on the details of the empirical model used for calculations. Ref. 17 found very significant variations of the stiffness with the radius of nanotubes when using the Tersoff inter-atomic potential and much smaller with the Brenner potential, *ab initio* calculations[10] also indicate a weak R-dependence of the stiffness. Molecular dynamics simulations of Ref. 6 yield ~ 0.05 for the ratio (32) for a very small tube (4,2).

One could expect a much larger stretch-induced torsion effect in the tubes which are elastically anisotropic already in the unwrapped sheet state. An example of such may be type-II BC_2N tubes, see Fig. 7, where an anisotropy is expected by virtue of the different inter-atomic interactions between different types of atoms. We therefore restrict our attention to η_0 term. As is clear from Fig. 7, the symmetry element left on the parent sheet is the reflection around the AB axis. Using this as a general symmetry constraint, one derives the anisotropic part of the elastic energy as

$$\begin{aligned} \delta U_{\rm m} &= C^a_0\gamma_0(\gamma\cos 2\phi_1 + \eta\sin 2\phi_1) \\ &+ \frac{C^a_{\rm sh}}{2}\left[(\gamma^2-\eta^2)\cos 4\phi_1 + 2\gamma\eta\sin 4\phi_1\right], \quad (34) \end{aligned}$$

where $\phi_1 = \phi - \pi/6$ and C^a_0 and $C^a_{\rm sh}$ are some anisotropy energies. Optimizing $U_{\rm m}$ now for a given $\gamma_\parallel$ and small anisotropy leads to the following chiral dependence of the effect:

$$\eta/\gamma_\parallel = -\left[(1-\nu)C^a_0\sin 2\phi_1 + (1+\nu)C^a_{\rm sh}\sin 4\phi_1\right]/2C_{\rm sh}. \quad (35)$$

It follows from (35) that the torsional shear vanishes for $\phi = \pi/6$ and $\phi = 2\pi/3$, that is, along respectively AB and OB vectors in Figure 7, as one could expect. In addition, the system may have another couple of such directions depending on the anisotropy parameters. The latter determine the sign and magnitude of the torsion. Some information on elastic properties of BC_2N tubes is available from *ab initio* calculations[18] but not sufficient for us to make estimates.

Torsion of nanotubes can also be caused by hydrostatic-like forces that would result in the isotropic lattice expansion/contraction in the absence of the anisotropy. One can find equilibrium η for a given γ_0 describing the isotropic effect. With the curvature-derived anisotropy energy (31) of carbon nanotubes, a finite η appears only in the second order of the anisotropy parameters:

$$\eta/\gamma_0 = (C^a_0 C^a_{\rm sh}/C^2_{\rm sh})\sin 6\phi,$$

and, therefore, is expected to be minuscule. In contrast, the inherent anisotropy energy (34) of BC_2N tubes leads to a finite effect already in the first order:

$$\eta/\gamma_0 = -(C^a_0/C_{\rm sh})\sin 2\phi_1,$$

and could be observable.

VII. SUMMARY

We have developed a simple framework for an effective description of the static lattice deformations for the hexagonal atomic structure of carbon nanotubes as well as of the actuation responses related to those deformations. Nanotubes present a potential to be used for various (nanoscale) actuators. It would suffice to mention the quasi-1-d geometry of individual tubes and the high surface area morphology of their assemblies, which e.g. leads to large electrochemical charge injection.[3] What is more, the very nature of the responses in nanotubes can provide unique opportunities.

Shear (anisotropic) deformations play an important role in nanotubes leading to large and fascinating deviations from the parent graphite behavior. It has been recognized that anisotropic deformations may introduce a symmetry breaking[12] and modulate the gap energy[8] in nanotubes. We have shown that charge injection can conversely result in shear deformations that would significantly increase the dimensional changes. Charge-induced strains exhibit a strong "oscillatory" dependence on nanotube geometry (N, M). The differences with isotropic graphite responses is predicted to be particularly large for semiconducting tubes at low injection levels. Large anisotropy of dimensional changes is expected, possibly leading in some cases to decreasing diameter and increasing length upon charge injection. For the same sign of carrier injection, some tubes may experience a longitudinal expansion while other a contraction. The same type of oscillatory dependence is also predicted for the charge-induced torsional deformations, that is, for the direction of the resulting twist. Even the electronic band structure of the nanotubes can reveal itself through sharp changes of the actuation responses upon changing the charge injection level. We found that the peculiar oscillatory behavior of the semiconducting tubes' responses

can be easily understood in terms of the bonding pattern which changes with $N - M$.

The best candidates to observe the enhanced dimensional responses would be semiconducting zigzag tubes. On the other hand, charge-induced torsional deformations should be best observable in semiconducting chiral nanotubes. However, an oscillatory dependence on $N-M$ will probably make the observation of the (larger) effects difficult. For a bundle of nanotubes of various geometries, experiments are likely to show some average, with strains from various semiconducting tubes "compensating" each other. Separation of semiconducting nanotubes of optimal type is therefore required to make the predicted enhancement practically useful.

The curvature-induced isotropy breaking of elastic interactions in carbon nanotubes also leads to a specific coupling of shear deformations and gives rise to another type of actuation - conversion of the tensile strain into torsion in chiral tubes. We believe such an actuation can be even more effectively achieved by using other types of nanotubes where anisotropy of elastic interactions is intentionally introduced through substitution of carbon atoms.

Within our framework, the model outputs depend on the values of several parameters such as effective elastic constants and electron-lattice interaction constants, for which we used some reasonable estimates. We however feel that a systematic comparison of the outputs to results of *ab initio* calculations and experimental data on graphite and nanotubes may also provide an alternative access to the microscopic parameters in these systems. It is remarkable that the symmetry of interactions in nanotubes imposes very definite requirements on the chirality dependence of the effects we discussed. It means that establishing values of the parameters for armchair and/or zigzag nanotubes will provide answers for tubes of arbitrary chirality.

VIII. ACKNOWLEDGEMENTS

This work was supported by DARPA Grant MDA972-02-C-005. We are grateful to M. Kertesz for drawing our attention to the graphite data. YNG is grateful to S. Lee for his help with references.

[1] R. Saito, G. Dresselhaus, and M. Dresselhaus, *Physical Properties of Carbon Nanotubes* (Imperial College Press, London, 1998).

[2] M. Dresselhaus, G. Dresselhaus, and P. Avouris, eds., *Carbon Nanotubes: Synthesis, Structure, Properties and Applications* (Springer, Berlin, 2000).

[3] R. Baughman, A. Zakhidov, and W. deHeer, Science **297**, 787 (2002).

[4] R. Baughman, C. Cui, A. Zakhidov, Z. Iqbal, J. Barisci, G. Spinks, G. Wallace, A. Mazzoldi, D. DeRossi, A. Rinzler, et al., Science **284**, 1340 (1999).

[5] Y. Gartstein, A. Zakhidov, and R. Baughman, Phys. Rev. Letters **89**, 045503 (2002).

[6] R. Baughman, A. Maiti, Y. Gartstein, R. Lakes, A. Zakhidov, and M. Kozlov, Science (submitted).

[7] Y. Miyamoto, A. Rubio, M. Cohen, and S. Louie, Phys. Rev. B **50**, 4976 (1994).

[8] L. Yang and J. Han, Phys. Rev. Letters **85**, 154 (2000).

[9] J. Lu, Phys. Rev. Letters **79**, 1297 (1997).

[10] D. Sánchez-Portal, E. Artacho, J. Soler, A. Rubio, and P. Ordejón, Phys. Rev. B **59**, 12678 (1999).

[11] G. Sun, J. Kürti, M. Kertesz, and R. Baughman, J. Amer. Chem. Soc. (to be published).

[12] C. Kane and E. Mele, Phys. Rev. Letters **78**, 1932 (1997).

[13] C. Chamon, Phys. Rev. B **62**, 2806 (2000).

[14] M. Verissimo-Alves, R. Capaz, B. Koiller, E. Artacho, and H. Chacham, Phys. Rev. Letters **86**, 3372 (2000).

[15] M. Kertesz, in *Intercalated Graphites*, edited by M. Dresselhaus (Elsevier, 1983), p. 141.

[16] S. Hong and M. Kertesz, Phys. Rev. Letters **64**, 3031 (1990).

[17] D. Robertson, D. Brenner, and J. Mintmire, Phys. Rev. B **45**, 12592 (1992).

[18] E. Hernández, C. Goze, P. Bernier, and A. Rubio, Phys. Rev. Letters **80**, 4502 (1998).

[19] Several combinations of elastic constants appear throughout the paper and we introduce their definitions here: $Z_{ab} = K_A K_B - K_{AB}^2$, $z_{ab} = K_A + K_B - 2K_{AB}$, $z_a = 2(K_B - K_{AB})/z_{ab}$ and $z_b = 2(K_A - K_{AB})/z_{ab}$.

[20] These considerations include symmetry requirements imposed by the following transformations: 1) nanotube axis inversion, $\phi \to \phi+\pi$; 2) reflection about the $y-$axis accompanied by $\phi \to -\phi$; 3) rotation by $2\pi/3$. The results we use correspond to the first term of the Fourier expansion in the angular dependence.

[21] Note that here we correct the expression incorrectly shown in Ref. 5.

[22] The curvature expansion contains only even powers of $1/R$ because this is the way all distances and scalar products of vectors modify when associated with atoms on a curved surface.

[23] The fact that $\delta\phi_l$ contains only odd powers of the curvature $1/R$ satisfies our notion that both these quantities are in fact associated with vectors/directions. Evidently, the torsion would happen in opposite directions when the parent horizontal sheet is wrapped upward vs downward to form a nanotube. On the other hand, the curvature-induced strain energy density[1,17] and anisotropy of the elastic interactions have to be independent of the wrapping direction and therefore are even functions of $1/R$.